Measurement of $2s$ and $3s$ electron spin densities at the iron nucleus in Fe_2O_3

T. Yang,* A. Krishnan, and N. Benczer-Koller
Department of Physics, Rutgers University, New Brunswick, New Jersey 08903
(Received 26 March 1984)

The $2s$ and $3s$ contributions to the core polarization at the nuclear site of ^{57}Fe in Fe_2O_3 films was measured by internal-conversion electron Mössbauer spectroscopy with a new high-transmission, high-resolution electrostatic electron spectrometer. The spin-density ratios $\delta_{ns} = |\psi_{ns}^{\uparrow}(0)|^2 / |\psi_{ns}^{\downarrow}(0)|^2 - 1$, $\delta_{2s} = -0.0048(7)$, and $\delta_{3s} = +0.0149(33)$ were determined.

I. INTRODUCTION

Twenty-five years ago the Mössbauer effect was discovered and has since then provided the means for detailed studies of remarkably diverse phenomena. In particular, the fortunate combination of the very narrow linewidths and the large hyperfine magnetic field in iron led to the first direct observation of the Zeeman effect in nuclei. The measurements of magnetically split nuclear levels initiated a new era of investigations of the hyperfine fields at a variety of nuclei embedded in magnetic materials, yielding a wealth of detailed information on the electronic interactions in such solids. Marshall[1] and Watson and Freeman[2] pioneered the theoretical understanding of the effective magnetic hyperfine field at the nucleus. In particular, they pointed out that the total hyperfine field is a sum of classical terms (external, demagnetizing, and Lorentz fields) and quantum-mechanical effects. The latter comprise the microscopic contributions from the contact interaction of the nucleus with s electrons in the Mössbauer atom itself, from the atomic electrons orbital angular momenta and dipolar fields, as well as from conduction electrons in the solid and from the dipolar or transferred hyperfine fields produced by neighboring atoms. In transition elements, the core-polarization term dominates; furthermore, for insulators in S states, the orbital field and the conduction-electron contribution vanish completely. The core-polarization component of the interaction is itself a sum of separate contributions from individual s electrons in each atomic shell. The standard recoilless absorption experiments, however, yield a measurement of the *total* magnetic hyperfine interaction. A microscopic experiment which combines Mössbauer with conversion electron spectroscopy was designed[3] to observe separately the *individual* contributions to the core polarization. The results of that experiment demonstrated the validity of the underlying assumptions of the Freeman and Watson model of core polarization and confirmed the predictions regarding the magnitudes and sign of s-shell contributions to the hyperfine interaction.

In order to improve the accuracy of the measurements and to perform a quantitative comparison with detailed theoretical models of the solid, a new spectrometer with high transmission and resolution was built. The results of the new experiment are described below and the potential and limitations of the technique are described.

II. CORE POLARIZATION AND THE FERMI CONTACT FIELD IN IRON ATOMS, IRON IONS, AND IRON METAL

Core s electrons in transition elements are polarized by the spin-dependent exchange interaction with the polarized d electrons. As a consequence of this polarization an effective magnetic field is produced at the nucleus, the well-known Fermi contact field:

$$\vec{H}_e = \frac{8\pi}{3} g\mu_B \vec{S} \sum [\,|\psi_{ns}^{\uparrow}(0)|^2 - |\psi_{ns}^{\downarrow}(0)|^2\,] , \qquad (1)$$

where $|\psi_{ns}^{\uparrow\downarrow}(0)|^2$ is the density at the nucleus of electrons in a given ns shell with spin parallel ($\uparrow$) or antiparallel ($\downarrow$) to the net d-electron spin, $\vec{S}$ is the net electronic spin in any given ion, and the summation is carried out over all shells. Watson and Freeman[2] have applied the unrestricted (spin- or exchange-polarized) Hartree-Fock (UHF) technique to calculate the contributions of the paired s electrons to the effective hyperfine field. Electron wave functions are obtained as self-consistent orthonormal eigenfunctions of the Hartree-Fock equation without requiring the radial part of the wave function to be spin independent. This technique involves the difficult task of calculating with high precision the difference between two terms of nearly equal magnitude. Nevertheless, this approach was exploited by Bagus and Liu[4] and Morita[5] for the case of the iron atom in the ^5D state.

Alternately, the restricted Hartree-Fock wave functions, for which the radial components are indeed spin independent, can be used as a set of orthonormal wave functions and the contact hyperfine field can be introduced as a perturbation.[6] The perturbed orbitals, $\psi'_{ns} = \psi_{ns} + \delta\psi_{ns}$, should satisfy the Hartree-Fock equations. Therefore, in the Hartree-Fock perturbation theory (HFPT), a set of $\delta\psi_{ns}$ is chosen to be orthogonal to the orbital wave function ψ_{ns}. In this approach, the difference between spin-up and spin-down orbitals, $\delta\psi_{ns}$, is obtained directly so that the problem of obtaining the difference between large and very nearly equal terms does not arise. In the self-consistent-field perturbation-theory calculation[7] (SCFPT), $\delta\psi_{ns}$ is written as a linear combination of zero-order orbitals. The linked-cluster many-body perturbation theory[8] (LCMBPT) uses the restricted Hartree-Fock Hamiltonian to generate a complete set of states and takes the difference between this Hamiltonian and the exact Hamiltonian

as a perturbation.

Band theory was introduced to calculate the spin density for iron metal. Wakoh and Yamashita[9] calculated the wave functions of the core states of metallic iron by the variational method in the unrestricted Hartree-Fock formulation while the wave functions of the band states are fixed. The band structure was determined by the Green's-function method. The wave functions of the band states are not completely orthogonal to those representing the core states, but the authors believe that the effect of the orthogonalization is not appreciable.

Callaway and Wang[10] used a linear combination of atomic orbitals (LCAO) with a basis consisting of independent Gaussian functions to calculate the spin density at the nuclear site. They employed two different kinds of potential, a local-exchange potential with two values of the strength parameter α [$\alpha=\frac{2}{3}$, the Kohn-Sham-Gaspar (KSG) values, and $\alpha=0.64$, an empirically chosen value] and a von Barth–Hedin exchange-correlation potential (vBH).

While these diverse sets of wave functions seem to yield approximately correct total hyperfine fields, they differ considerably in their shell-by-shell predictions and experimental data are needed to indicate the proper approach.

In order to facilitate the comparison with experimental data and with other calculations, the quantities χ_{ns} and δ_{ns} must be evaluated:

$$\chi_{ns}=\frac{4\pi}{2S}[\,|\psi^{\uparrow}_{ns}(0)|^2-\psi^{\downarrow}_{ns}(0)|^2]\,. \tag{2}$$

χ_{ns} is given in atomic units and represents the effective field per unpaired electron; $2S$ is the number of localized electrons in the $3d$ shell. Hence,

$$\delta_{ns}=[\,|\psi^{\uparrow}_{ns}(0)|^2/|\psi^{\downarrow}_{ns}(0)|^2]-1 \tag{3}$$

is the quantity that is most readily measured. The resulting hyperfine field can be obtained from χ_{ns} and δ_{ns} by using the conversion factor 1 a.u.$=4.21$ T, and an estimate of the appropriate charge density of the individual s electrons at the nucleus

$$H_{ns}=(4.21)\chi_{ns}2S=4\pi(4.21)\frac{\delta_{ns}}{\delta_{ns}+2}\rho_{ns}(0)\ \text{T}\,, \tag{4}$$

where

$$\rho_{ns}(0)=[\,|\psi^{\uparrow}_{ns}(0)|^2+|\psi^{\downarrow}_{ns}(0)|^2]$$

is the total ns electron charge density.

The theoretical calculations were carried out for iron metal or the iron atom in the ^5D state which have 2.2 and 4 unpaired $3d$ electrons, respectively, while Fe_2O_3 has 5 unpaired $3d$ electrons. The calculated spin densities were henceforth normalized by the appropriate ratio of unpaired $3d$ electrons to relate to the case of Fe_2O_3. This procedure would certainly not be valid for valence electrons, but may not be too far off for core electrons which are less affected by the chemical environment. It is, however, the only approach available to compare theory to experiment in the absence of calculations specific to Fe_2O_3.

Several calculations of s-electron charge densities $\rho_{ns}(0)$ are summarized in Table I. In contrast to the theoretical estimates of spin densities, all calculations of charge densities of core electrons agree within a few percent. Thus the contact fields resulting from the net spin density of individual s shells can be estimated without ambiguity. The charge densities calculated by Freeman and Ellis[11] for the Fe^{3+} ion were combined with the measured spin densities to determine the hyperfine magnetic fields corresponding to $2s$ and $3s$ spin polarization.

The resulting χ_{ns}, δ_{ns}, and effective hyperfine fields for the various calculations are summarized in Table II and are compared to the experimental results. A negative sign of the spin density corresponds to a net electron spin at the nucleus antiparallel to the net spin of the $3d$ electrons, while a negative hyperfine field points in a direction antiparallel to the $3d$-electron magnetization.

TABLE I. Electron charge densities (in atomic units).

		Bagus and Liu (Ref. 4)	Freeman and Ellis (Ref. 11)	Wakoh and Yamashita (Ref. 9)	Callaway and Wang (Ref. 10) vBH	KGS	$\alpha=0.64$
	$\lvert\psi^{\uparrow}_{1s}(0)\rvert^2$	5386.490			5195.79	5166.28	5163.45
$1s$	$\lvert\psi^{\downarrow}_{1s}(0)\rvert^2$	5386.537			5195.83	5166.41	5163.58
	$\frac{\lvert\psi^{\uparrow}_{1s}(0)\rvert^2+\lvert\psi^{\downarrow}_{1s}(0)\rvert^2}{2}$	5386.514	5387.596	5377.68	5195.81	5166.35	5163.52
	$\lvert\psi^{\uparrow}_{2s}(0)\rvert^2$	493.668			472.07	469.86	468.96
$2s$	$\lvert\psi^{\downarrow}_{2s}(0)\rvert^2$	496.213			472.82	470.72	469.79
	$\frac{\lvert\psi^{\uparrow}_{2s}(0)\rvert^2+\lvert\psi^{\downarrow}_{2s}(0)\rvert^2}{2}$	494.940	95.429	493.87	472.45	470.29	469.38
	$\lvert\psi^{\uparrow}_{3s}(0)\rvert^2$	68.587			68.661	68.367	68.261
$3s$	$\lvert\psi^{\downarrow}_{3s}(0)\rvert^2$	67.162			68.152	67.834	67.749
	$\frac{\lvert\psi^{\uparrow}_{3s}(0)\rvert^2+\lvert\psi^{\downarrow}_{3s}(0)\rvert^2}{2}$	67.874	68.966	68.94	68.407	68.101	68.005

TABLE II. Calculated spin densities, $\delta_{ns}=\frac{|\psi^{\uparrow}_{ns}(0)|^2}{|\psi^{\downarrow}_{ns}(0)|^2}-1$, of core s electrons at the ^{57}Fe nucleus, hyperfine magnetic fields per spin, χ, and hyperfine magnetic field at the nucleus, H(T), for Fe_2O_3.

Electron-shell theory	1s δ	1s χ	1s H (T)	2s δ	2s χ	2s H (T)	3s δ	3s χ	3s H (T)	$H_{1s+2s+3s}$ (T)
Atomic structure calculation										
UHF (Ref. 4)	−0.000011	−0.15	−3.2	−0.0064	−7.99	−168.2	0.0265	4.48	94.3	−77.1
HFPT (Ref. 6)	0.000009	0.12	2.5	0.0030	−3.78	−79.6	−0.0246	−0.42	−8.8	−85.9
SCFPT (Ref. 7)	−0.000004	−0.06	−1.3	−0.0062	−7.69	−161.9	0.0223	3.80	80.8	−83.2
LCMBPT (Ref. 8)	0.000001	0.02	0.4	0.0028	−3.47	−70.3	−0.0040	−0.69	−14.5	−84.4
Fe^{3+}-ion calculation										
UHF (Ref. 4)	−0.000018	−0.25	−5.3	−0.0068	−8.51	−179.1	0.0339	5.77	121.5	−62.9
HFPT (Ref. 6)	0.000007	0.10	2.1	−0.0035	−4.50	−94.7	0.0045	0.79	16.6	−76.0
SCFPT (Ref. 7)	−0.000010	−0.14	−3.0	−0.0071	−8.88	−186.9	0.0317	5.41	113.9	−76.0
LCMBPT (Ref. 8)	0.000003	0.04	0.8	−0.0035	−4.37	−92.0	0.0030	0.52	11.0	−80.2
Band theory										
Wakoh and Yamashita (Ref. 9)	−0.000011	−0.15	−3.2	−0.0064	−7.98	−168.0	0.0241	4.28	90.1	−81.1
vBH	−0.000018	−0.23	−4.8	−0.0036	−4.23	−89.0	0.0170	2.91	61.2	−32.6
Callaway and Wang KSG (Ref. 10) $\alpha=0.64$	−0.000057	−0.73	−15.4	−0.0042	−4.92	−103.6	0.0179	3.05	64.2	−54.8
	−0.000055	−0.70	−14.7	−0.0040	−4.73	−99.6	0.0172	2.92	61.5	−52.8

Experiment	2s δ	2s H (T)	3s δ	3s H (T)	H_{2s+3s} (T)
Previous work (Ref. 3)	−0.0063(24)	−164.4(62.6)	0.0217(88)	77.0(31.2)	−87.4(70.0)
Present work	−0.0048(7)	−126.1(18.4)	0.0149(33)	54.0(12.0)	−72.1(22.0)
					H (total)
Transmission Mössbauer spectroscopy					−51.76(0.01)

III. THE DETECTION OF SPIN DENSITY OF S ELECTRONS AT THE NUCLEUS IN Fe-BASED MAGNETIC MATERIALS

The basic idea behind these measurements has been described in detail in previous publications.[3] Only an overview will be presented here.

The 14.4-keV, $\frac{3}{2}^+$, excited state of ^{57}Fe decays to the $\frac{1}{2}^+$ ground state by an $M1$ transition which is heavily converted with an internal conversion coefficient $\alpha = 8.26 \pm 0.19$. In a magnetic material, the nuclear levels are split into $m_I = I, \ldots, -I$ components. In $M1$ internal conversion, the decay proceeds mainly by emission of s electrons. The intensity of the transition is proportional to the charge density of s electrons at the nucleus, $\alpha^{\uparrow(\downarrow)} \approx |\psi_{ns}^{\uparrow(\downarrow)}(0)|^2$. The change in angular momentum $\Delta I = 1$ is carried away by the emitted electrons. The initial s electron has an $s_{1/2}$ configuration and is emitted into an $s_{1/2}$ or $d_{3/2}$ final state, with the $\Delta l = 0$ transition being about 10 times more probable than the $\Delta l = 2$ transition. For the $\Delta l = 0$ transition to proceed, emitted electrons must flip their spin, so that the $\Delta m_I = -1$ transition can only occur by emission of s electrons with original spin down with respect to the magnetization of the $3d$ shell and the $\Delta m_I = +1$ transition involves emission of electrons with initial spin up. These concepts are illustrated in Fig. 1. The selection of electrons with appropriate spin is experimentally done by Mössbauer spectroscopy, while the selection of electrons from individual s shells is carried out with the aid of a high-resolution electron spectrometer. The energies of the internal-conversion electrons emitted from $1s(K)$, $2s(L_I)$, and $3s(M_I)$ shells are 7.3, 13.6, and 14.3 keV, respectively.

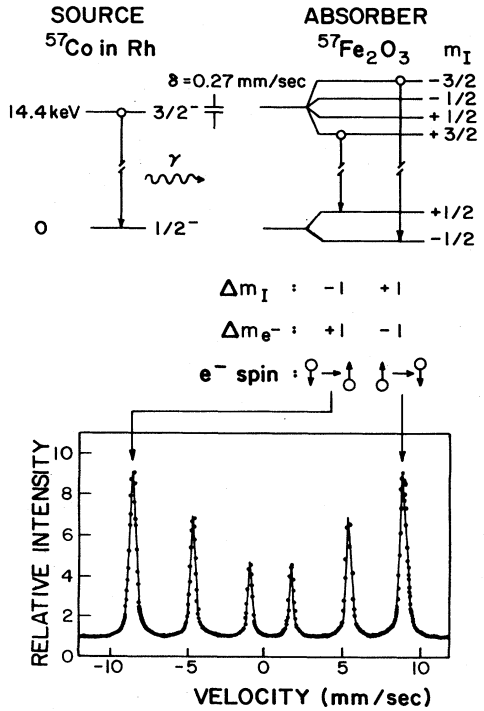

FIG. 1. Energy level diagram of ^{57}Fe embedded in magnetic (Fe_2O_3) matrices indicating the $\Delta m_I = 1$ transitions, the corresponding Mössbauer spectrum, and the change in angular momentum of the internally converted electrons.

Thus the measurement of the spin density of s electrons necessitates the selective excitation of the $m_I = +\frac{3}{2}$ and $m_I = -\frac{3}{2}$ substates of ^{57}Fe by recoilless absorption of 14.4-keV γ rays emitted from a nonmagnetic, unsplit, source of ^{57}Co in a Rh matrix. The decay conversion electrons are energy selected by the electron spectrometer. The measured ratio of electrons corresponding to the two Zeeman transitions,

$$R_{ns} = \frac{N^-(m_I = \frac{3}{2} \rightarrow \frac{1}{2})}{N^+(m_I = -\frac{3}{2} \rightarrow -\frac{1}{2})},$$

is directly related to the ratio of spin densities at the nuclear site for s electrons in each ns subshell,

$$|\psi_{ns}^{\uparrow}(0)|^2 / |\psi_{ns}^{\downarrow}(0)|^2 .$$

IV. EXPERIMENT

The experiment was carried out with ^{57}Co(Rh) sources which were moved by an electromechanical transducer in a special velocity mode that emphasizes the Zeeman lines of interest. Thin-film absorbers of Fe_2O_3 were positioned at the "source" position of an electron spectrometer. The details of the apparatus are described below.

A. Electron spectrometer

The electron spectrometer, a spherical electrostatic condenser, was especially designed for experiments in Mössbauer conversion electron spectroscopy.[12] In particular, the diameter of the electron source can be made as large as 1 cm without loss of resolution. The characteristics and details of the construction are described elsewhere.[12] Figure 2 shows a schematic of the instrument. This particular design was chosen because its geometry is

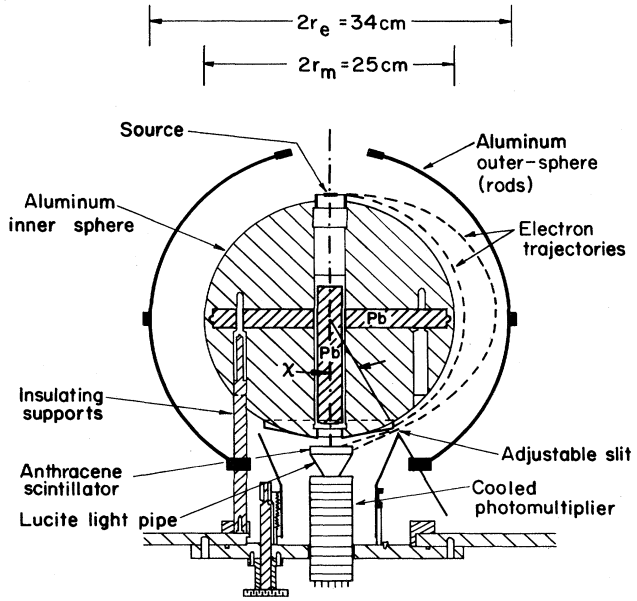

FIG. 2. Schematic of the electrostatic spherical electron spectrometer.

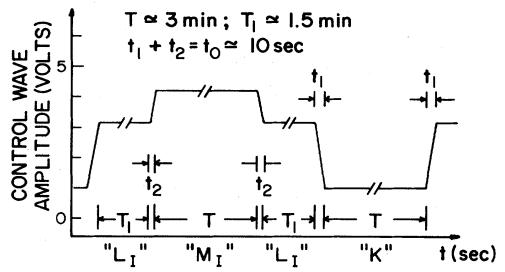

FIG. 3. Control waveform used to vary the electron spectrometer potential in order to scan sequentially over the K, L_I, and M_I portions of the conversion electron spectrum.

especially suitable for the positioning of sources and absorbers in Mössbauer spectroscopy and because such a spectrometer is capable of fairly high transmission, $T=13\%$, at an adequate energy resolution $R=\Delta E/E=2\%$.

The electron detector consisted of an anthracene film which was brushed from a benzene solution on a Lucite cylinder, 5 cm in diameter and 1 cm long. A thin (20 $\mu g/cm^2$) Formvar film was deposited over the anthracene face to prevent evaporation of the scintillator. To improve the signal-to-noise ratio, a cone-shaped light pipe of 5 cm upper diameter and 3 cm lower diameter, was optically interfaced between the lucite cylinder and a cooled Amperex 56DVP photomultiplier. A small negative voltage, -5 to -10 V, applied to the focus electrode acted to further reduce the effective area of the photocathode and hence the dark noise. The Formvar foil also served to stop very-low-energy secondary electrons, thus improving the signal-to-noise ratio.

To obtain electron spectra, a negative high voltage was applied to the outer sphere. The calibration constant of the spectrometer was $E_0/V=1.650$, where E_0 is the energy of electrons that would be focused for an applied voltage V.

When the spectrometer is used in conjunction with the Mössbauer drive, an additional potential V_s proportional to V must be applied to the lead collimator surrounding the Mössbauer source in order to compensate for the field distortion introduced by the source holder assembly. V and V_s were produced by regulated power supplies which were externally controlled by either a digitized triangular waveform or a multistep constant voltage waveform generator (Fig. 3). The first scheme was used for display of the complete energy spectrum. The second system was used in conjunction with the velocity drive to obtain Mössbauer spectra for fixed electron energies. In this latter mode, the spectrometer setting was changed with a period of the order of minutes over up to three different voltages. The voltage switching was synchronized with the velocity reference waveform. The corresponding spectra were stored in different quadrants of a 4096-channel analyzer.

B. Velocity transducer

The transducer, based on a design by Genard-Riondet,[13] consists of two mechanically coupled loudspeaker magnets with the coils (drive coils) wired in parallel. The

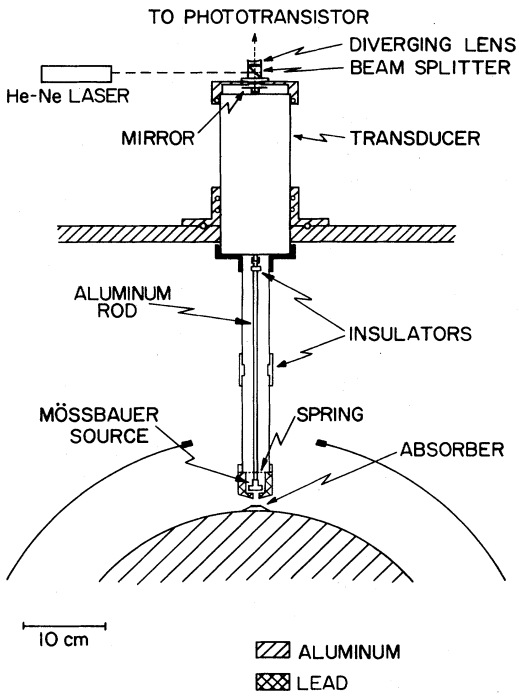

FIG. 4. Schematic of the arrangement of the Mössbauer drive, source, and absorber at the source end of the spectrometer.

pickup coil from a Schaevitz 6L1VT-Z velocity transducer was used to measure the instantaneous velocity of the drive. A long aluminum rod holding the Mössbauer source was attached to the transducer and was centered by an external flat spring mounted on a lead collimator. The system was operated at 10 Hz.

The velocity response of the signal was continuously monitored during the whole experiment by means of a Michelson interferometer. The light beam from a He-Ne laser was aimed at a mirror attached to the back of the velocity transducer and the interference fringe pattern between the beam reflected from the moving mirror and the beam scattered by the beam splitter (Fig. 4) was detected by a phototransitor, operation amplifier, and Schmitt trigger. The light signal was thus transformed into pulses that were fed to the first quadrant of the multichannel analyzer.

C. Velocity waveform

Two different velocity patterns could be generated: (i) a standard triangular waveform with which the whole Mössbauer pattern could be displayed [Figs. 5(a) and 5(b)]; (ii) a specific velocity spectrum whereby the outer lines were emphasized at the expense of the low-velocity inner lines [Figs. 5(c) and 5(d)].

The first scheme was used to test the chemical purity and physical condition of the absorbers. The usual six-line pattern characteristic of Fe_2O_3 was observed as a function of the spectrometer voltage corresponding to electron energies 6.5, 7.0, 7.3, 13.6, and 14.3 keV, respectively. In all cases the intensity ratios and the isomer shift were the same and no impurity resonances showed up

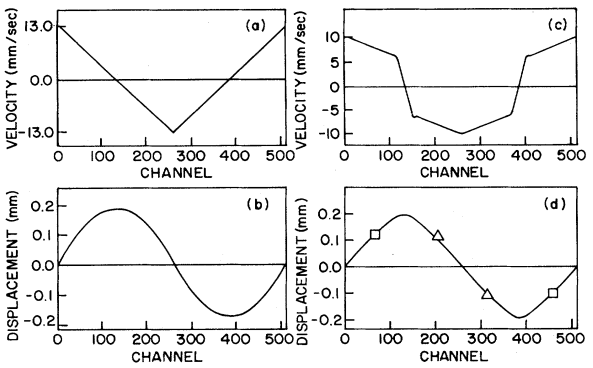

FIG. 5. Velocity spectra measured by Michelson interferometry and corresponding source displacements obtained by integration of the velocity spectra. (a) and (b) correspond to a linear velocity scan, while (c) and (d) represent the velocity waveform used to emphasize the outer lines in the Mössbauer spectrum. The squares and triangle correspond to the position of the source for positive and negative velocity, respectively.

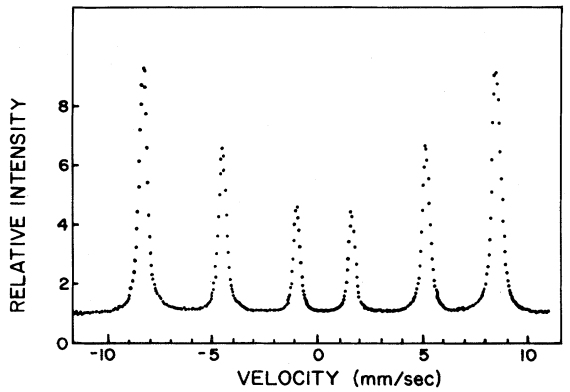

FIG. 6. Mössbauer K-conversion electron spectrum obtained with a linear velocity waveform.

anywhere in the spectrum. The special velocity waveform was designed to select the lines of interest and thus enhance the total counting rates. In addition, this particular mode results in a displacement pattern such that the *average* source-absorber distance corresponding to equal positive- or negative-velocity regions is that of the equilibrium position and more important, is the *same* for both positive- and negative-velocity regions. This configuration is most readily shown graphically by the squares and triangles in Fig. 5(d). Thus the geometrical asymmetries that were inherent in the previous experiment are eliminated in first order. As a test of the geometry, Mössbauer spectra of the background electron spectrum were measured with the electron spectrometer set well above 14.4 keV, the highest internal conversion line. A value of the ratio of backgrounds at negative and positive velocity $B^-/B^+=0.9981\pm0.0012$ was obtained, confirming the absence of instrumental asymmetry arising from the unusual motion of the drive.

D. Sources and absorbers

Single-line ^{57}Co sources in a Rh matrix with a thickness of 10 μm were used. The sources' strength varied from 100 to 40 mCi and the activity was concentrated over an area of 2×2.5 mm.[14] Mössbauer spectra taken with natural iron absorbers 30 μm thick, indicated that these sources had a recoilless fraction of $f\simeq0.76$ and a linewidth $\Gamma_s=0.169$ mm/sec. The α-Fe_2O_3 absorber was prepared by evaporation of an enriched (90%), 100 μg/cm^2, 1 cm diameter, ^{57}Fe film onto a 0.04 cm thick sapphire substrate in a vacuum of 10^{-5} Torr. The film was first annealed in hydrogen (99.999% purity) at 1000 K for 4 h. Subsequently, it was oxidized at 100 K for 4 h in pure oxygen and was quenched to room temperature. The quenching procedure prevents formation of γ-Fe_2O_3.

Figure 6 shows a Mössbauer—K-conversion electron spectrum for this sample. The source-absorber distance d was adjustable; values of $d=2.0$ and 2.5 cm were used with 40-, 50-, and 80-mCi sources, respectively. Typical counting rates for the latter configuration are shown in Table III.

E. Electron spectra

The internal conversion spectra obtained from the Fe_2O_3 absorber in the "source" position of the spectrometer is shown in Fig. 7. Spectra were measured both on- and off-resonance and the net spectra were obtained by subtraction of these two. The K, L, and M electrons are clearly resolved, and Mössbauer spectra were obtained by setting the spectrometer alternately on or near the peak of each line.

It was discovered in the course of these experiments, that when the spectrometer is set on the peak of the K electron distribution, electrons from the surface of the sample are preferentially transmitted. Electrons from the interior lose energy while emerging from the sample and appear in the low-energy tail of the K line. It was also noted that the hyperfine interaction is smaller at the surface of the film than in the bulk.[15] In the measurement of the spin density of $L_I(2s)$ and $M_I(3s)$ electrons, the $K(1s)$ electrons were used to calibrate the instrument for geometrical asymmetries because it is expected that their net

TABLE III. Typical counting rates of internal conversion electrons. Source ^{57}Co(Rh): 80 mCi; absorber α-Fe_2O_3: 100 μg/cm^2; source-absorber distance $d=2.5$ cm.

Electron shell	Net signal at resonance counts/sec	Background counts/sec	Signal background
K	260	50	5.2
L	160	55	2.9
M	30	45	0.7

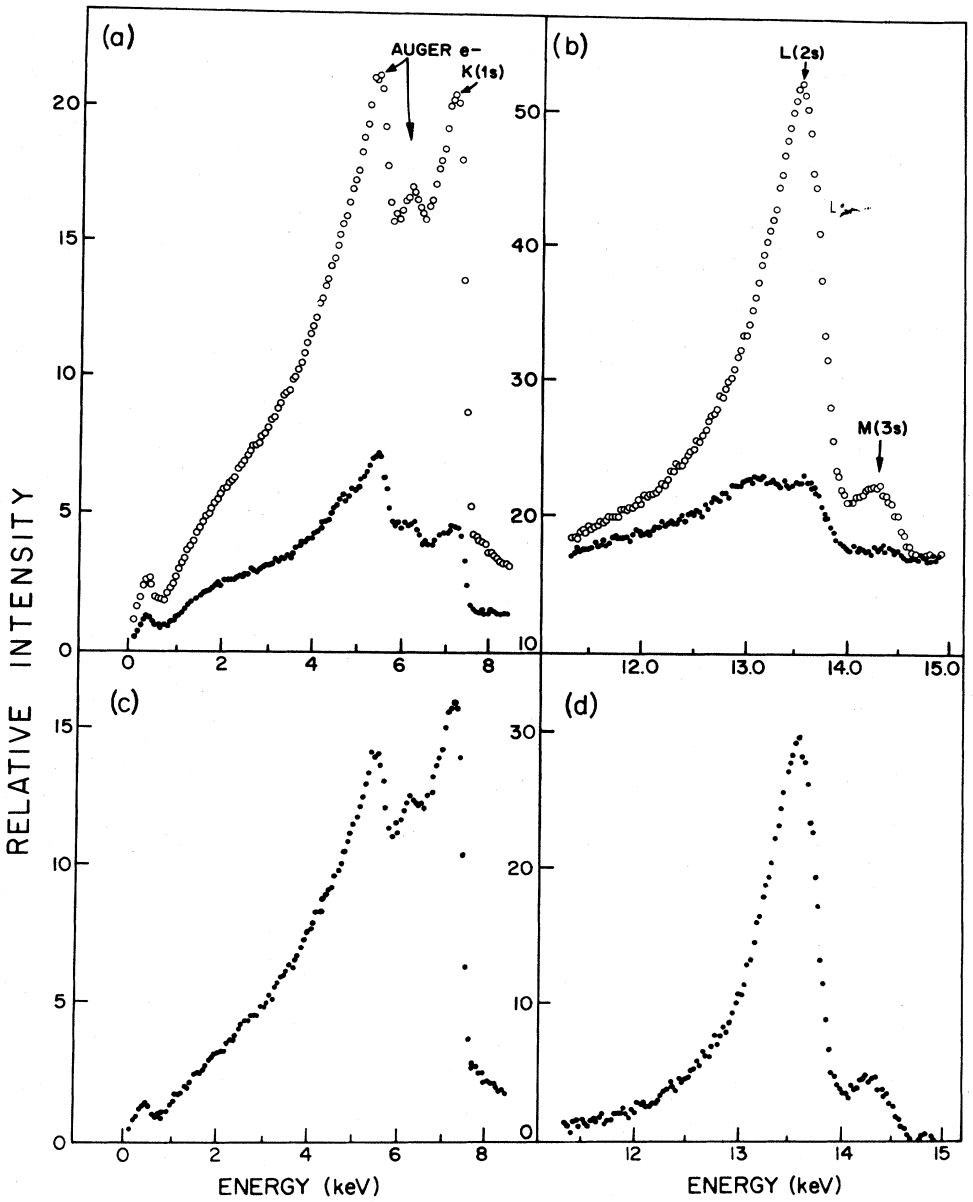

FIG. 7. (a) Low-energy and (b) high-energy internal conversion electron spectra obtained on- and off-resonance (background and external conversion) are indicated by the open and solid circles, respectively. The net on-resonance internal-conversion spectra resulting from the subtraction of the off-resonance data from the on-resonance yield are shown in (c) and (d).

spin density is extremely small. It is important to use as normalization K electrons that originate in the bulk as do most of the $2s$ and $3s$ electrons and therefore the spectrometer was set at 6.9 keV rather than on the peak of the K-electron line.

F. Mössbauer spectra

The transducer was operated in the special velocity mode that enhances the outer lines. The electron spectrometer was stepped every 3 min over three electron energies. The Mössbauer spectra were independently stored in three quadrants of the multichannel analyzer. A typical spectrum is shown in Fig. 8(a) plotted against channel and in Fig. 8(b) plotted against velocity. The velocity is obtained from the interferometer data stored in the first quadrant.

TABLE IV. Values of $R_K=(N_K^-/N_K^+)$ for different K-electron energies.

Electron energy (keV)	R_K
7.3	0.9916(11)
7.2	0.9905(8)
7.15	0.9912(13)
6.9	0.9903(10)
6.5	0.9898(15)

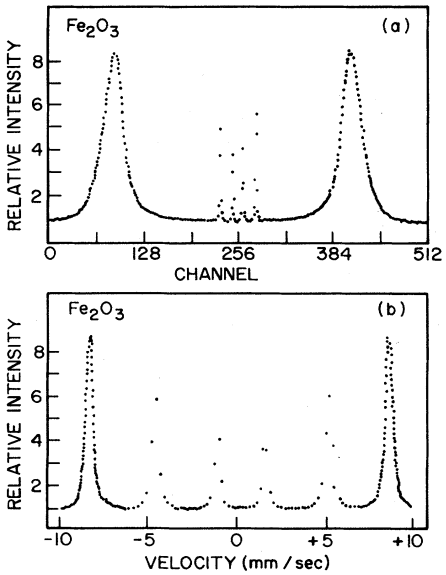

FIG. 8. K—internal-conversion spectra obtained with the special waveform emphasizing the lines of interest plotted against (a) the channel number and (b) the source velocity.

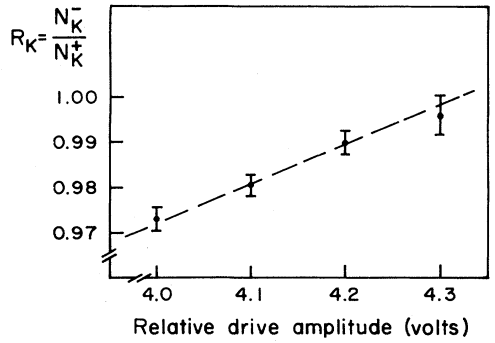

FIG. 9. Ratio of the negative-to-positive—velocity yields of K-electrons measured as a function of the amplitude of the velocity waveform. This plot points to the importance of comparing only ratios N_i^-/N_i^+ ($i=K$, L_I, and M_I) obtained with the *same* velocity waveform.

V. DATA AND ANALYSIS

The data were analyzed by first subtracting the off-resonant background from the spectra. The background was determined by fitting the off-resonance channels to a constant. The ratios of the areas under the positive- and negative velocity peaks $R_i=N_i^-/N_i^+$ ($i=K$, L_I, or M_I) were calculated by choosing the same number of channels for the peaks. The ratio R_K should be essentially equal to unity because the $1s$ electrons, having small overlap with the d electrons are barely affected by the net d-electron spin and are expected to have a very small spin density. Most calculations predict $\delta_{1s}<10^{-4}$ (Table II). Thus, the data for $2s$ and $3s$ electrons were normalized to the data for the $1s$ electrons in order to correct for whatever geometrical or instrumental asymmetries might exist in the experiment. For example, because the slopes of the velocity for the two could be slightly different (it is not possible to adjust the drive amplitude exactly with the required precision), the average source-absorber solid angles could be different for the positive and negative velocities.

The deviation of the ratio R_K, from unity, was measured as a function of the setting of the velocity amplitude. The results, plotted in Fig. 9 emphasize the importance of measuring the L_I and M_I electrons at the same setting as that used for the K electrons. In the original experiment, carried out with a long lens-solenoid magnetic spectrometer, geometrical asymmetries resulted in a 10% variation in the counting rates at the opposite velocities; in the present experiments, however, the ratios R_K were very close to unity, thus reducing considerably possible systematic errors.

Table IV shows typical values of R_K for a particular source-absorber geometry, as a function of electron energy. It is clear that for a given setting of the velocity amplitude, not only are the counting rates corresponding to the two velocities almost equal, but the ratios R_K are also independent of the electron energy. Table V shows the ratios R_K, R_L, and R_M obtained for different sources and different source-absorber distances.

Finally, having ascertained that the $K(1s)$ electrons can be used to normalize out the geometrical effects, the ratios R_L and R_M were divided by R_K in order to determine the spin densities for the $L_I(2s)$ and $M_I(3s)$ electrons.

In order to obtain the spin-density ratios δ_{ns} from the data, the ratios R_{ns} must be corrected for the fact that the resolution of the spectrometer is insufficient to resolve the

TABLE V. Typical values of $R_i=(N_i^-/N_i^+)$, $i=K$, L, and M, and the ratios R_i/R_K for different sources and geometries.

	R_K	R_L	R_M	R_L/R_K	R_M/R_K
$d=2.0$ cm, 50 mCi	0.9883(6)	0.9853(7)	1.0019(45)	0.9969(10)	1.0138(49)
$d=2.5$ cm, 80 mCi	0.9854(10)	0.9809(11)	1.0010(60)	0.9953(15)	1.0158(64)
$d=2.5$ cm, 40 mCi	0.9956(29)	0.9891(39)	1.0151(173)	0.9935(49)	1.0196(176)
$d=2.5$ cm, 80 mCi	0.9944(8)	0.9896(7)		0.9951(10)	
	0.9887(10)	0.9837(13)		0.9950(16)	
	0.9902(15)		1.0012(94)		1.0111(96)
	0.9878(8)	0.9847(10)	0.9981(43)	0.9969(13)	1.0104(44)
Average				0.9956(7)	1.0105(40)
AVERAGE				0.9959(6)	1.0128(28)

TABLE VI. Spin densities $\delta_{ns} = |\psi^{\uparrow}_{ns}(0)|^2/|\psi^{\downarrow}_{ns}(0)|^2 - 1$, of $2s$ and $3s$ electrons at the Fe nucleus in Fe_2O_3.

	δ_{2s}	δ_{3s}
Previous work	-0.0063 ± 0.0024	0.0217 ± 0.0088
This work		
$d=2.0$ cm, 50 mCi	-0.0037 ± 0.0012	0.0161 ± 0.0057
$d=2.5$ cm, 80 mCi	-0.0055 ± 0.0018	0.0184 ± 0.0075
$d=2.5$ cm, 40 mCi	-0.0077 ± 0.0058	0.0229 ± 0.0205
$d=2.5$ cm, 80 mCi	-0.0052 ± 0.0009	0.0122 ± 0.0047
Average	-0.0048 ± 0.0007	0.0149 ± 0.0033

L_{II}, L_{III}, and $M_{II}, \ldots, M_V$ internal-conversion electrons from the L_I and M_I electrons. The ratios $N_{L_I}/(N_{L_{II}}+N_{L_{III}})=10.7\pm0.1$ and $N_{M_I}/(N_{M_{II}}+\cdots+N_{M_V}) = 12.08\pm0.26$ were used[16,17] and the spin densities δ_{ns} were calculated from the following expressions:

$$\frac{R_L}{R_K}=1+\frac{\delta_{2s}}{1+[(N_{L_{II}}+N_{L_{III}})/N_{L_I}](2+\delta_{2s})}$$

and

$$\frac{R_M}{R_K}=1+\frac{\delta_{3s}}{1+[(N_{M_{II}}+\cdots+N_{M_V})/N_{M_I}](2+\delta_{3s})}\ .$$

Table VI shows the spin densities obtained in the four different runs, the average of all data, as well as the results of the previous experiment.

VI. DISCUSSION

This experiment yields a direct measurement of the ratios of spin-up to spin-down densities of $2s$ and $3s$ electrons and an indirect measurement of the contact hyperfine fields at the nuclear site contributed by the net spin density of the $2s$ and $3s$ subshells.

The data are to be compared to theoretical predictions based on the models described in Sec. II. The measured spin densities δ_{2s} and δ_{3s} agree with the sign but certainly not with the magnitude predicted by either the atomic structure, the Fe^{3+} ion, or Wakoh and Yamashita's iron metal band-structure calculations.

On the other hand, the calculations of Callaway and Wang appear to be in very good agreement with experiment. However, their calculation might not represent Fe_2O_3 adequately, because the crystal structure and electronic potential used in the calculation are appropriate to iron metal and may not be suitable to the case of an ionic crystal where the outer s-electron wave functions are probably distorted by electrostatic fields of near neighbors or other ligand effects. These distortions may affect the spin densities more than the charge densities. Nevertheless, because the $4s$ electrons at iron in Fe_2O_3 are shared with the oxygen ions, a situation similar to that in iron metal where the $4s$-electron electrons in the conduction band and itinerant $3d$ electrons are shared by other iron atoms, may prevail. On balance, the calculation provides a very good *qualitative* picture of the hyperfine fields contributed by each individual core s electron for each unpaired $3d$ electron. This result could be anticipated since from the microscopic point of view, the inner core s electrons ought not be affected much by differences of structure and environment which affect mostly the valence electrons.

In addition, relativistic correlations may be important. The calculations displayed in Tables I and II are nonrelativistic. According to Mallow *et al.*,[18] the solutions of the Dirac equation lead to a value of the effective charge density $|\rho_s(0)|^2$ at the nuclear site for s states in iron or iron compounds as much as 30% larger than the values obtained in a nonrelativistic calculation. Unfortunately, relativistic spin-density calculations are not available yet.

It is interesting to note that while all calculations predict a value of the "total" hyperfine field at the nucleus in reasonable agreement with experiment, it is the microscopic measurement of the individual contributions that have the sensitivity that allows for a detailed scrutiny of the theoretical procedures.

Further interpretation of the present measurements will have to await for relativistic calculations of Fe_2O_3 wave functions. Similar measurements on iron-metal films are in progress.

ACKNOWLEDGMENTS

This work was supported in part by the National Science Foundation. We wish to express our thanks to Dr. T. Kachnowski and Dr. B. Kolk for their extensive contributions in the early stages of this experiment.

*Present address: Physics Department, Emory University, Atlanta, GA 30322.

[1]W. Marshall, Phys. Rev. **110**, 1280 (1958).

[2]R. E. Watson and A. J. Freeman, Phys. Rev. **120**, 1125 (1960); **120**, 1134 (1960).

[3]C. J. Song, J. Trooster, N. Benczer-Koller, and G. M. Rothberg, Phys. Rev. Lett. **29**, 1165 (1972); C. J. Song, J. Trooster, and N. Benczer-Koller, Phys. Rev. B **9**, 3854 (1974).

[4]P. S. Bagus and B. Liu, Phys. Rev. Lett. **4**, 513 (1960).

[5]M. Morita, K. Sugimoto, M. Yamada, and Y. Yokoo, Prog. Theor. Phys. **41**, 996 (1969).

[6]K. J. Duff and T. P. Das, Phys. Rev. **168**, 43 (1968).

[7]K. J. Duff and T. P. Das, Phys. Rev. B **3**, 2294 (1971); **12**, 3870 (1975).
[8]T. Lee, N. C. Dutta, and T. P. Das, Phys. Rev. A **1**, 995 (1970); S. N. Ray, Taesul Lee, and T. P. Das, Phys. Rev. B **8**, 5291 (1973); H. Kelly and A. Ron, Phys. Rev. A **2**, 1261 (1970).
[9]S. Wakoh and J. Yamashita, J. Phys. Soc. Jpn. **25**, 1272 (1968).
[10]J. Callaway and C. S. Wang, Phys. Rev. B **16**, 2095 (1977); R. A. Tawil and J. Callaway, *ibid.* **9**, 4897 (1974).
[11]A. J. Freeman and D. E. Ellis, in *Mössbauer Isomer Shifts,* edited by G. K. Shenoy and F. E. Wagner (North-Holland, Amsterdam, 1978).
[12]T. S. Yang, B. Kolk, T. Kachnowski, J. Trooster, and N. Benczer-Koller, Nucl. Instrum. Methods **197**, 545 (1982).
[13]N. Genard-Riondet, P. Inbert, and J. F. Lericque, Rev. Sci. Instrum. **49**, 606 (1978).
[14]The ^{57}Co(Rh) sources were prepared by Amersham Corp.
[15]T. Yang, A. Krishnan, N. Benczer-Koller, and G. Bayreuther, Phys. Rev. Lett. **48**, 1292 (1982).
[16]F. T. Porter and M. S. Freedman, Phys. Rev. C **3**, 2285 (1971).
[17]T. Shinohara and M. Fujioka, Phys. Rev. B **7**, 37 (1973).
[18]J. J. Mallow, A. J. Freeman, and J. P. Desclaux, Phys. Rev. B **13**, 184 (1976).